A&A, 709, A91 (2026)
https://doi.org/10.1051/0004-6361/202557908

Astronomy & Astrophysics

Very high-energy gamma rays from ultra-fast outflows

B. Le Nagat Neher[1,⋆], E. Peretti[2,3], P. Cristofari[1], and A. Zech[1]

[1] LUX, Observatoire de Paris, Université PSL, Sorbonne Université, CNRS, 92190 Meudon, France
[2] INAF, Istituto Nazionale di Astrofisica, Osservatorio Astronomico di Arcetri, Largo E. Fermi 5, 50125 Florence, Italy
[3] APC, Université Paris Diderot, CNRS/IN2P3, CEA/Irfu, Observatoire de Paris, Sorbonne Paris Cité, France

Received 30 October 2025 / Accepted 8 March 2026

ABSTRACT

Context. Ultra-fast outflows (UFOs) from active galactic nuclei (AGNs) are expected to lead to the formation of sub-relativistic strong shocks expanding in a dense, circumnuclear medium, and thus have the potential to be efficient particle accelerators and proficient sources of gamma rays and neutrinos.
Aims. We aim to investigate the detectability of a sample of nearby identified UFOs in gamma rays and neutrinos with current and next-generation instruments.
Methods. We modeled the acceleration of particles at the strong shocks of UFOs and estimated the associated gamma-ray and neutrino signal. We adopted our model to investigate the prospects for detection with current and next-generation observatories.
Results. We find that several UFOs could be detectable in the very-high-energy (VHE) domain – for example, by the Cherenkov Telescope Array Observatory (CTAO) – even if they remain undetected by *Fermi*-LAT in the high-energy range. Detectability is favored for hard proton spectra (spectral index $\alpha \lesssim 3.9$), high acceleration efficiencies, and amplified magnetic fields. Our results suggest that next-generation VHE observatories could detect the first gamma-ray signatures of AGN UFOs, providing a new probe of particle acceleration in sub-relativistic shocks.

Key words. acceleration of particles – gamma rays: general

1. Introduction

Active galactic nuclei (AGNs) are powered by accretion onto supermassive black holes, and they are considered to play a role in feedback on galaxies (Silk & Rees 1998). Thanks to advances in X-ray spectroscopy, fast ionized outflows were detected more than 20 years ago (Pounds et al. 2003; Reeves et al. 2003). These outflows have been identified after observations of blueshifted Fe absorption lines (Chartas et al. 2002; Cappi et al. 2009).

The typical distances on which these outflows expand span from fractions of a parsec to tens of parsecs from the supermassive black holes (Gianolli et al. 2024), with typical velocities of $v \geq 0.1$c and a wide range of mass-loss rates: $\dot{M} \approx 10^{-4}$–$100\,\mathrm{M_\odot\,yr^{-1}}$. Wind velocities up to $v \approx 0.4$c have been observed by Gofford et al. (2013), and even a record measurement at $v = 0.76$c has been reported (Chartas et al. 2009). Such high velocities led to these winds being dubbed ultra-fast outflows (UFOs; Tombesi et al. 2010; King & Pounds 2015). UFOs are indeed sub-relativistic winds launched with a wide opening angle, within which shocks can form, typically as a consequence of their fast expansion in the interstellar medium (ISM). Regardless of the AGN class, radio-loud (jetted, Tombesi et al. 2014) or radio-quiet (Tombesi et al. 2012) UFO detections with common properties (Mestici et al. 2024) have been observed. This suggests that UFOs may be relatively common in AGNs, independent of the presence of a co-existing jet. The launching mechanisms of UFOs remain unclear. They could be radiation-driven (Jiang et al. 2014) or magnetically driven outflows (Fukumura et al. 2010, 2014; Gianolli et al. 2024). The geometry and the environments of AGN-driven winds have been explored by Faucher-Giguère & Quataert (2012) and Nims et al. (2015), among others. However, the details of the circumnuclear medium properties in which UFOs expand are still little known.

The physical conditions met at UFOs, in particular their high speed and kinetic power, make them particularly suited for diffusive shock acceleration (DSA), with the formation of strong, sub-relativistic collisionless shocks in a dense medium. The energization of particles at least up to the very high-energy (VHE) domain is expected, in turn, to lead to the production of gamma rays and neutrinos in the high-energy (>1 GeV) and VHE ranges (>1 TeV). Observational support for particle acceleration in UFOs has come from a stacking analysis of 11 selected UFO hosts with *Fermi*-LAT (*Large Area Telescope*) (Ajello et al. 2021). This work showed that UFOs are a class of gamma-ray emitters.

A definitive detection of UFOs in the gamma-ray domain remains elusive. The nearby UFO host NGC 4151 is spatially consistent with a *Fermi*-LAT source (Murase et al. 2024; Peretti et al. 2025), hinting at possible gamma-ray emission from the UFO, though the association is not yet beyond doubt due to a possible contamination from a blazar at 5 arcmin. NGC 1068, despite its high column density, is also a plausible UFO host detected in the GeV range. However, the origin of such gamma rays is highly uncertain due to the co-existence of many possible acceleration sites such as star-forming regions (Yoast-Hull et al. 2014; Eichmann et al. 2022; Ajello et al. 2023), an AGN molecular outflow (Lamastra et al. 2016, 2019), and a mildly relativistic radio jet (Lenain et al. 2010; Salvatore et al. 2024; see also Padovani et al. 2024 for a detailed review). More than 15 years of *Fermi*-LAT monitoring has otherwise yielded upper limits to individual UFO hosts. UFOs have also been proposed and

⋆ Corresponding author: baptiste.le-nagat-neher@obspm.fr

studied as potential sources of ultra-high-energy cosmic rays observed at Earth (Peretti et al. 2023; Ehlert et al. 2025). Here, we studied the gamma-ray and neutrino emissions for a list of selected UFOs, reported after the detection of blueshifted absorption lines of highly ionized iron in their X-ray spectrum obtained with *XMM-Newton* (Ehlert et al. 2025), whose physical properties are summarized in Fig. 1.

We discuss the prospects for detection with current and next-generation observatories, for gamma rays and for neutrinos. In this work, we focused on an order-of-magnitude discussion, which encompasses all shocks developed throughout the UFO expansion, and on the prospects for detection in gamma rays in the GeV, TeV, and 100 TeV ranges, accounted for by the typical sensitivities of *Fermi*-LAT, the CTAO (*Cherenkov Telescope Array Observatory*), and LHAASO (*Large High Altitude Air Shower Observatory*) (Atwood et al. 2009; Acharya et al. 2019; Neronov & Semikoz 2020). We focused on the hadronic component of the gamma-ray emission. The leptonic contribution is expected to be subdominant in the conditions relevant for UFOs. On the one hand, the high ambient densities ($\sim 10^2$–10^5 cm^{-3}; Laha et al. 2019; Ricci & Trakhtenbrot 2023) strongly enhance the efficiency of hadronic interactions and subsequent π^0-decay gamma-ray production. On the other hand, the magnetic fields inferred for these environments lead to severe synchrotron losses for relativistic electrons, limiting both their maximum attainable energy and their radiative efficiency in the gamma-ray domain. Moreover, a leptonic gamma-ray component strong enough to dominate would inevitably imply bright synchrotron counterparts from radio- to X-ray wavelengths, which are generally not observed in association with such outflows. As a result, the hadronic channel is expected to provide the dominant contribution to the high-energy emission.

Regardless of the cases of NGC 4151 and NGC 1068, UFOs have not been clearly detected by *Fermi*-LAT (Abdollahi et al. 2020). We aim to investigate UFO contributions in the TeV range that could be detectable by the CTAO, typically offering a tenfold improvement in TeV range sensitivity over current atmospheric Cherenkov telescopes. The prospects for detection in neutrinos is discussed considering the sensitivity of KM3NeT/ARCA (*Astroparticle Research with Cosmics in the Abyss*) (Aiello et al. 2024), not forgetting that an analogous comparison could be done with IceCube-Gen2 (Aartsen et al. 2021).

The manuscript is organized as follows. In Sect. 2 we introduce the framework of our investigation describing the main scalings of UFOs and the computation of the associated gamma-ray and neutrino fluxes. In Sect. 3 we present our results on the UFO detectability with gamma rays and neutrinos. We discuss our findings and draw our conclusions in Sect. 4.

2. Gamma rays and neutrinos from UFOs

2.1. Particle acceleration at UFOs

The launching of UFOs driven by AGNs is expected to lead to the formation of strong shocks (Mach number $\mathcal{M} \gg 1$). In the initial phase, the outflow freely expands into the surrounding circumnuclear medium, leading to the formation of a forward shock (FS). The deceleration of the wind material due to the collision with the external medium gives rise to the formation of a second shock, i.e. the wind termination shock (TS), inside the wind structure. These two shocks are coupled in the first stages of the dynamics of the wind. When the swept-up external medium material balances the wind mass itself, the expansion slows down and the pressure equilibrium leads to the decoupling

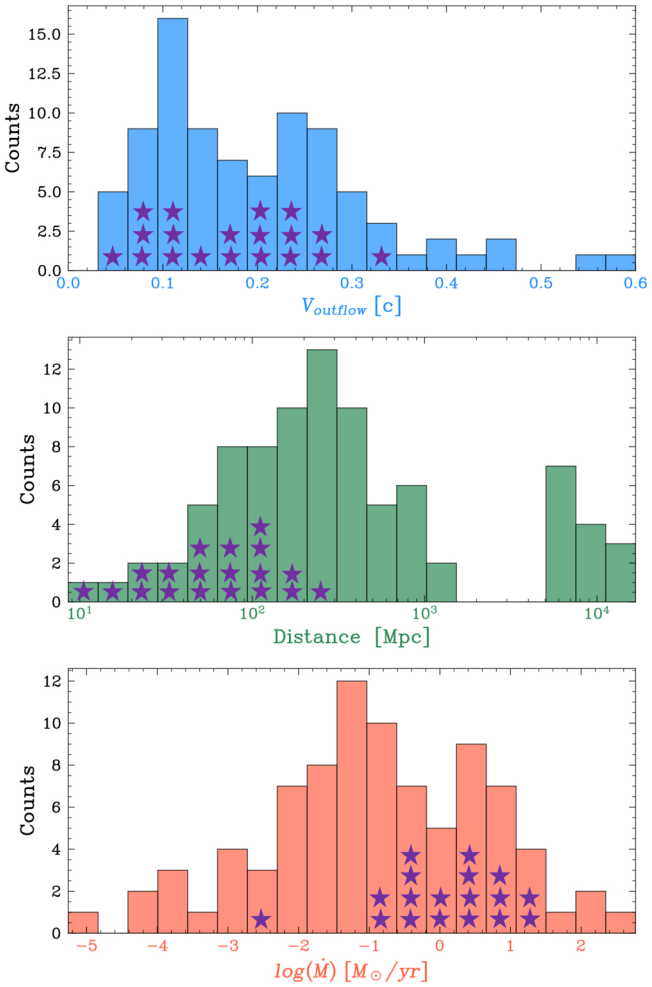

Fig. 1. Description of the sample of sources: distributions of the outflow speed (top), distance (middle), and mass-loss rate (bottom). Violet stars indicate the main properties of the detectable UFOs, which are summarized in Table 2.

of the two shocks (Weaver et al. 1977; Chevalier & Clegg 1985). The deceleration time, $t_{\rm dec}$, at which this happens reads as

$$t = t_{\rm dec} \implies \dot{M}t = \frac{4\pi}{3} R_{\rm FS}^3(t)\rho_0, \tag{1}$$

where $\dot{M}$ is the mass outflow rate, $R_{\rm FS}$ is the FS radius, and ρ_0 is the density of the surrounding medium. We stress that our model does not describe the propagation of a single observed UFO clump from sub-parsec scales out to distances of 1–10 pc. Rather, we assume that the kinetic power injected by the outflow drives strong collisionless shocks in the surrounding circumnuclear medium. The characteristic size of the shock region is treated as a free parameter, reflecting the uncertain geometry and dynamical evolution of the wind-ISM interaction. Importantly, the duration of an observed UFO episode does not determine the lifetime of the shock. Even a short-lived outflow as short as $t_{\rm obs} \sim 10^5$ s in PDS456 (Xu et al. 2025) can deposit sufficient kinetic energy to launch a shock that propagates over much longer timescales ($t_{\rm wind} \sim 10^4$ yr) and distances, as commonly observed in transient astrophysical systems (e.g., supernovae or novae). While the transient nature of UFO observations introduces uncertainty on the wind properties, the small dispersion of UFO characteristics reported in the literature across multiple observations of individual sources (e.g., Tombesi et al. 2010;

Matzeu et al. 2023; Chartas et al. 2021) indicates that even a single X-ray detection can provide meaningful insight into their potential as VHE gamma-ray emitters. Our treatment therefore models the long-term interaction between the integrated wind kinetic power and the ambient medium, rather than the direct propagation of an individual UFO clump to parsec scales. The deceleration time can thus be expressed as follows:

$$t_{\rm dec} \approx 56 \left(\frac{\dot{M}}{1 M_\odot/{\rm yr}}\right)^{1/2} \left(\frac{v_\infty}{0.1\ {\rm c}}\right)^{-3/2} \left(\frac{n_0}{100\,{\rm cm}^{-3}}\right)^{-1/2} \quad {\rm yr}, \tag{2}$$

where $n_0 = \rho_0/m_{\rm p}$ and v_∞ is the terminal wind speed.

If the source age satisfies $t_{\rm age} \lesssim t_{\rm dec,}$ the FS and TS remain coupled, and the former can be expected to be the only strong shock of the system. For $t_{\rm age} \gtrsim t_{\rm dec}$, they can be considered to be distinct, and, at late times ($t_{\rm age} \gg t_{\rm dec}$), the FS is expected to be slow and radiative, thus limiting particle acceleration up to the highest energies.

At these shocks, depending on the stage of the evolution, strong collisionless shock conditions can be found. Thus, DSA is expected to be efficient in energizing particles. Indeed, the high wind velocities, typically $\gtrsim$ 0.1c, ensure that in all dynamical phases, at least one shock's Mach number is $\mathcal{M} \gg 1$, while the shocks remain sub-relativistic, thereby allowing for particles to be injected efficiently in the acceleration process. A priori, particle acceleration at the TS and FS can differ, as the different acceleration conditions concur in setting the maximum momentum and the normalization of the accelerated particles.

Our modeling implicitly assumes that shocks form as the UFO interacts with the surrounding circumnuclear medium. While direct observational evidence for such shocks is still lacking, physical factors make their formation difficult to avoid. For an outflow with a characteristic velocity of $v_\infty \sim$ 0.1c, shock formation is indeed expected whenever the relative velocity exceeds the magnetosonic speed of the ambient medium, $v_{\rm ms} = (c_s^2 + v_A^2)^{1/2}$. Avoiding shocks would therefore require unusually extreme external conditions, such as temperatures of $T \sim 10^{10}$ K or magnetic-field strengths close to $B \sim 0.1$ G, which is higher than those typically inferred at circumnuclear scales (Zavala & Taylor 2004). In the absence of such conditions, the interaction between the UFO and its environment is expected to generically produce strong shocks. A schematic view of the geometry under consideration is shown in Fig. 2. To account for potential acceleration at both the FS and the TS, we normalized our spectrum using assumptions that can be easily translated from one case to the other.

As mentioned above, depending on the evolutionary stage of the UFO, one expects the FS or the TS to be the most relevant site for DSA. Therefore, we work under the assumption that DSA is at play at one shock, without distinguishing between the two. We consider that protons are accelerated through DSA and that their distribution follows a power law in momentum:

$$f(p) = A \left(\frac{p}{p_0}\right)^{-\alpha} \exp\left(-\frac{p}{p_{\rm max}}\right), \tag{3}$$

where α is the index of the spectrum and $p_{\rm max}$ is the maximum momentum deduced from the Hillas criterion (see discussion below). In the test-particle limit of DSA, at strong shocks $\alpha = 4$, but several nonlinear effects can lead to deviations from the test-particle case and produce harder or steeper spectra (Malkov & Drury 2001; Amato & Blasi 2005; Zirakashvili & Ptuskin 2008; Caprioli et al. 2020; Cristofari et al. 2022). The normalization A was obtained assuming that a fraction, $\xi_{\rm CR}$, of the fluid ram pressure at the shock, ρv_∞^2, is transferred to the pressure of accelerated particles: $P_{cr} = \frac{4\pi}{3} \int_{p_{\rm min}}^{p_{\rm max}} {\rm d}p\ p^3 v(p) f(p)$, where ρ is the density, $v(p)$ the particle velocity, and $p_{\rm min}$ and $p_{\rm max}$ the minimum and maximum momentum of accelerated particles. As long as $p_{\rm min} \lesssim m_{\rm p} c$, its precise value is not relevant for determining the cosmic rays (CR) pressure.

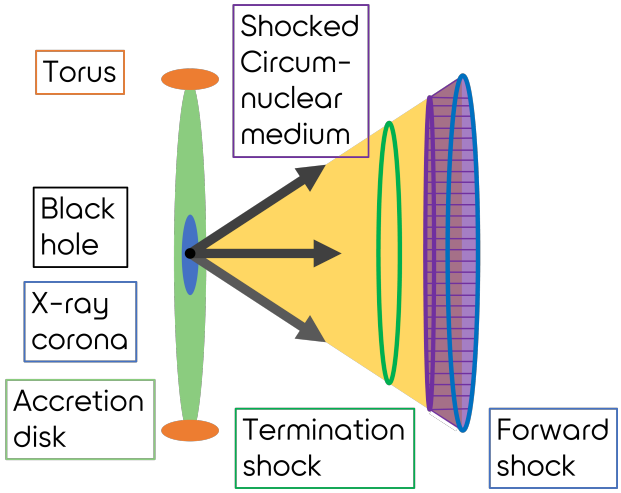

Fig. 2. Schematic representation of the geometry of UFOs and associated shocks.

The ram pressure at the FS and TS, respectively expanding in the external medium and in the dense UFO wind, read

$$P_{\rm ram}(t) = \begin{cases} m_{\rm p}\, n_0\, v_{\rm FS}^2 & [{\rm FS}] \\ \frac{\dot{M}}{4\pi\, R_{\rm TS}^2} v_\infty & [{\rm TS}], \end{cases} \tag{4}$$

where $R_{\rm TS}$ is the TS radius. We assumed that the UFO is sufficiently evolved such that the velocity of the TS satisfies $v_{\rm TS} \ll v_\infty$. The typical energy available at each shock can then be estimated by considering the volumes potentially filled with accelerated particles $4\pi R_{\rm TS}^2 l_{\rm TS}$ and $4\pi R_{\rm FS}^2 l_{\rm FS,}$ associated with the TS and FS, respectively, where $l_{\rm TS} \sim R_{\rm FS} - R_{\rm TS}$ and $l_{\rm FS} \sim R_{\rm FS} - 0.9 R_{\rm FS}$:

$$E \sim \begin{cases} 10^{54} \left(\frac{n_0}{100{\rm cm}^{-3}}\right) \left(\frac{v_{\rm FS}}{0.1\ c}\right)^2 \left(\frac{R_{\rm FS}}{3\ {\rm pc}}\right)^2 \left(\frac{l_{\rm FS}}{0.3{\rm pc}}\right) {\rm erg} & [{\rm FS}] \\ 10^{54} \left(\frac{\dot{M}}{1 M_\odot/{\rm year}}\right) \left(\frac{v_\infty}{0.1\ c}\right) \left(\frac{l_{\rm TS}}{3{\rm pc}}\right) {\rm erg} & [{\rm TS}]. \end{cases} \tag{5}$$

This illustrates that although the TS is often regarded as the primary site of particle acceleration, the FS can also contribute significantly, especially at early times. It should also be emphasized that the estimates in Eq. (5) are time dependent, but the temporal evolution is mild; for instance, at the FS one finds $E \propto t^{-2/5}$. Moreover, the strength of the FS is governed by the average properties of the external medium, and efficient radiative losses in the shocked ambient gas may cause the shock to become radiative. Although UFOs are observed to be transient and structured on short timescales near the central engine (Gu et al. 2025), such variability does not necessarily translate into rapidly evolving conditions at larger scales. The termination and FSs are governed by the time-averaged wind properties and evolve on dynamical timescales much longer than the events observed close to the central engine. We therefore adopted a steady-state description based on ranges of UFO parameters to model the associated VHE emission. In the following, we assume that particle acceleration occurs at a generic shock, without specifying whether it is the TS or the FS. The comparable energy budget of the two shocks (Eq. (5)) supports such

Table 1. Parameters of the model.

α	Slope of particles accelerated at the shock
ξ_{CR}	Efficiency of acceleration at the shock
ξ_B	Fraction of ram pressure transferred to magnetic field
n_0	Target material density
R_{sh}	Typical size of the accelerating region

an assumption and makes our results on the hadronic byproduct general. We characterized the size of this shock by its radius, R_{sh}, and consider that the accelerated particles occupy a volume corresponding to a fraction $\beta \simeq 0.5$ of the spherical volume $4\pi R_{sh}^3/3$. This region is taken to be responsible for the production of the resulting gamma-ray and neutrino emission.

At this shock, the maximum energy of accelerated particles is tightly connected to the level of magnetic field around the shock. In the presence of efficient acceleration, the streaming of accelerated particles is likely to play a crucial role in the excitation of instabilities in the plasma and to lead to a substantial amplification of the magnetic field, especially at FSs. While at TSs a high level of turbulence and magnetic-field amplification is naturally expected as a result of compression. Regardless of the process(es) at stake setting the average value of the magnetic field at the shock, we assume that a fraction ξ_B of the shock ram pressure is converted into magnetic-energy density (Miniati et al. 1999):

$$U_B = \frac{B^2}{8\pi} = \xi_B \rho v_\infty^2, \tag{6}$$

with $\xi_B \approx 10^{-4}$, typically resulting in magnetic-field values on the order of hundreds of μG.

We assumed a magnetic conversion efficiency somewhat lower than Peretti et al. (2023). This, besides resulting in a lower maximum energy for protons as discussed below, is for us a conservative assumption that allows the co-accelerated electrons not to cool too rapidly via synchrotron, thereby allowing for a potential contamination due to inverse Compton emission that we discuss in Sect. 3.

The associated maximum energy attainable through DSA is set by the Hillas criterion (Hillas 1984):

$$E_{max} \approx 38 \left(\frac{r_{sh}}{1\,pc}\right)^{-1} \left(\frac{v_\infty}{0.1\,c}\right) \left(\frac{\xi_B}{10^{-4}}\right) \left(\frac{\dot{M}}{0.1\,M_\odot/yr}\right) PeV. \tag{7}$$

Our conservative choice of a low ξ_B should not be interpreted as excluding UFOs as potential sources of ultra-high-energy CRs – indeed $0.01 < \xi_B < 0.1$ is compatible with $E_{max} \gtrsim 10^{18}$ eV – rather it reflects our focus on a pessimistic scenario regarding potential electron contamination in the gamma-ray domain via inverse Compton emission. Such contamination would, in fact, be suppressed by stronger synchrotron losses for larger ξ_B values.

The main parameters of our model are summarized in Table 1. Other physical quantities such as the mass-loss rate, velocity of the outflows, and distance of the UFO winds are taken from the literature (Ehlert et al. 2025).

2.2. Gamma rays and neutrinos

The interactions of accelerated hadrons with protons and nuclei of the circumnuclear medium (CNM) result in the production of neutral and charged pions. In turn, gamma rays result from the decay of neutral pions, while neutrinos are the final products, together with electrons and positrons, of the decay of charged pions. We do not distinguish between neutrino flavors as the oscillation en route to Earth results approximately in flavor equipartition. The corresponding emissions were computed following Kelner et al. (2006) and Kafexhiu et al. (2014).

The gamma-ray signal from pion decay was computed with the *Naima* code (Khangulyan et al. 2014; Kelner et al. 2006; Kafexhiu et al. 2014), assuming the proton distribution described by Eq. (3). We neglected the leptonic contamination to the gamma-ray flux, and we comment on the robustness of our assumption at the end of Sect. 3.

The gamma-ray signal can be substantially degraded due to the interaction of gamma rays with low-energy photons through the two-photon process, creating electron-positron pairs. The absorption is taken into account considering two distinct phases of the photon propagation: (1) in the production region, high-energy gamma rays interact with the AGN-background photon field; (2) outside the source, gamma rays interact with the photons of the cosmic microwave background (CMB) and of the extragalactic background light (EBL). To account for (1), three AGN photon-field components were considered as a combination of different black bodies corresponding to two physical parts of the AGN – the dusty torus ($\approx 10^3$ K Mullaney et al. 2011) and the accretion disk ($\approx 10^4$ K) – and a power law for the X-corona as in Marconi et al. (2004). The absorption on CMB and EBL depends on the redshift of the source, and we adopted the prescription described in Franceschini & Rodighiero (2017).

3. Results

The main goal of our work is to discuss the prospects of detection of UFOs in the gamma-ray domain with present and next-generation instruments such as the CTAO or LHAASO. We present the gamma rays and neutrinos expected for the list of 82 UFOs selected in Ehlert et al. (2025), following the methodology presented in the previous section.

Setting aside the previously discussed cases of NGC 1068 and NGC 4151, the lack of *Fermi*-LAT detections of UFOs is not straightforward to interpret. This could either indicate that the physical conditions in each source hinder GeV emission, or that, intrinsically, UFOs as a population are inefficient producers of GeV gamma rays. As the non-detection remained difficult to interpret, we adopted two approaches. In the first, we examined all sources individually and investigated the conditions in which they can be detected by CTAO while remaining undetected by *Fermi*. In the second, we studied the sample as a whole and explored the regions of parameter space that could lead to a CTAO detection, while remaining consistent with the non-detection of all UFOs by *Fermi*.

In our first approach, we performed an exploration of the parameter space (α, ξ_{CR}, n_0, R_{sh}, and B) and computed the gamma-ray and neutrino signal expected from each source. We focused on sources whose gamma-ray spectra exceed the sensitivity of the CTAO and remain below the sensitivity of *Fermi*-LAT to account for the fact that no clear UFO detection has been claimed by *Fermi*-LAT besides NGC 4151 and NGC 1068.

The number of expected UFOs for typical values of α, ξ_{CR}, and n_0 are illustrated in Fig. 3. We show (from top to bottom) three different assumptions for the external target density. On the left-hand side of each panel, we display the parameter space of the detectable sources. The expected gamma-ray and neutrino fluxes for the sources of interest are illustrated on the right sides. The typical differential sensitivities of *Fermi*-LAT,

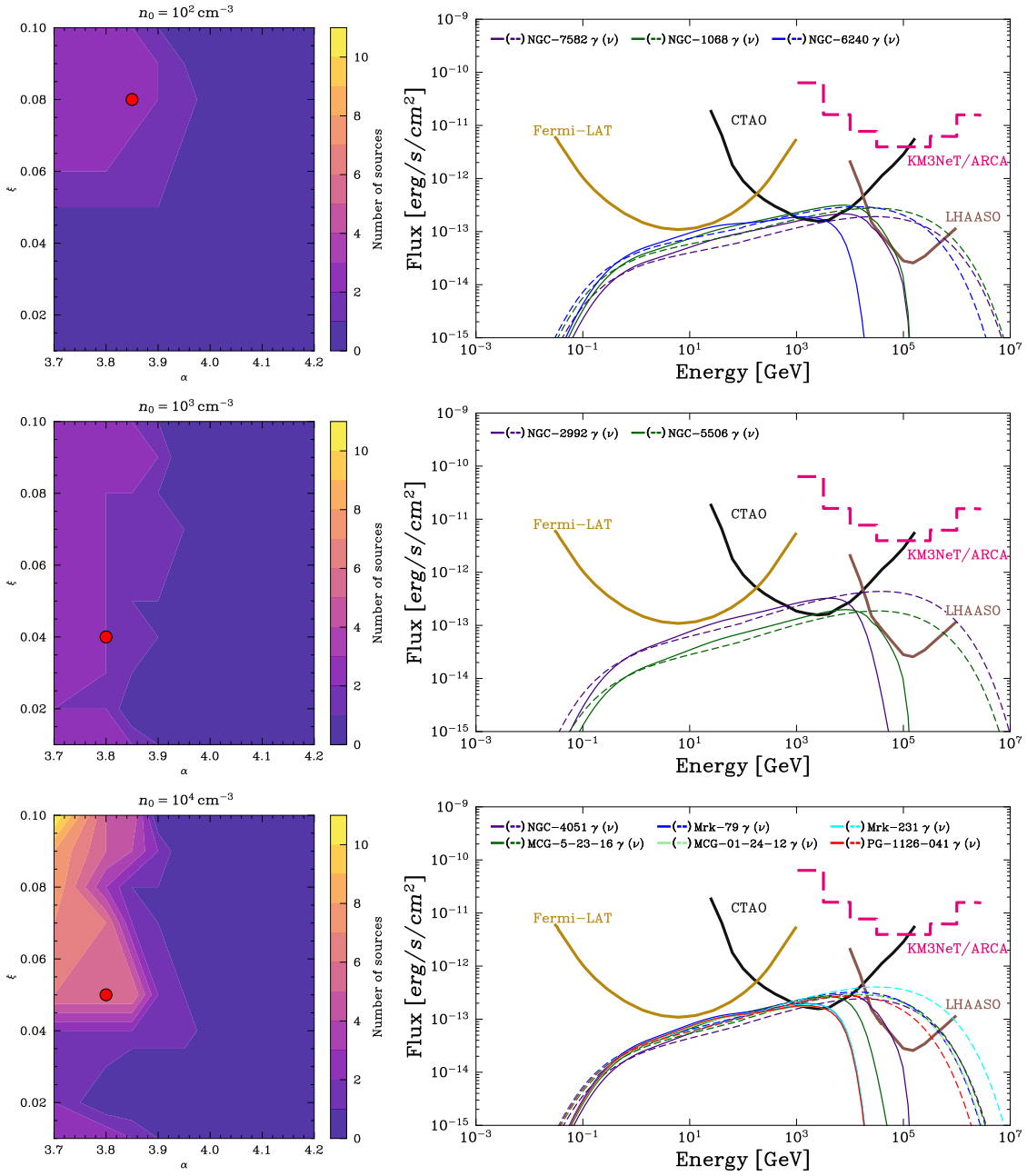

Fig. 3. Number of UFOs with a gamma-ray signal above the typical sensitivity of the CTAO (50 hours) and below the *Fermi*-LAT sensitivity. The shock radius is $R_{\rm sh} = 1$ pc. Panels from top to bottom illustrate different assumptions of external density: $n_0 = 10^2$–10^3–10^4 cm^{-3}. Sensitivities of *Fermi*-LAT (14 years), LHAASO (5 years) and KM3NeT/ARCA (10 years) are shown.

the CTAO, and the LHAASO are also displayed for comparison. In our sample of the best UFO candidates, an index of $\alpha \lesssim 3.9$ and an efficiency of $\xi_{\rm CR} \gtrsim 0.05$ led to at least one potential detection in the VHE domain, regardless of the value assumed for the target density, n_0. As expected, the number of expected sources increases with n_0, $\xi_{\rm CR}$, and $R_{\rm sh}$ (increasing the CR density and target density) and with harder spectra (smaller values of α).

In our second approach, we treated the sample of UFOs as a whole and investigated the regions of parameter space that could lead to a detection with CTAO, while remaining consistent with the fact that all UFOs are undetected with *Fermi*-LAT. Results are illustrated in Fig. 4. The difference between the two approaches can be seen by comparing the top panels of Figs. 3 and 4, which correspond to a size of the accelerating zone, $R_{\rm sh} = 1$ pc, and density, $n_0 = 10^2$ cm^{-3}.

Our second approach relies on a more drastic criterion, thus significantly reducing the number of detectable UFOs and the interesting regions of the parameter space for a detection in the VHE range. As shown in Fig. 4, even with this stricter criterion, several UFOs remain detectable across specific regions of the parameter space explored for both $R_{\rm sh} = 1$ pc and $R_{\rm sh} = 10$ pc.

Both approaches suggest that at least one UFO with a hadronic TeV component could be observable, while still being consistent with the lack of UFO detections in the GeV range. The best UFO candidates for a detection in the TeV range are reported in Table 2. The most promising sources are the nearest ones, for which the gamma-gamma absorption on the CMB

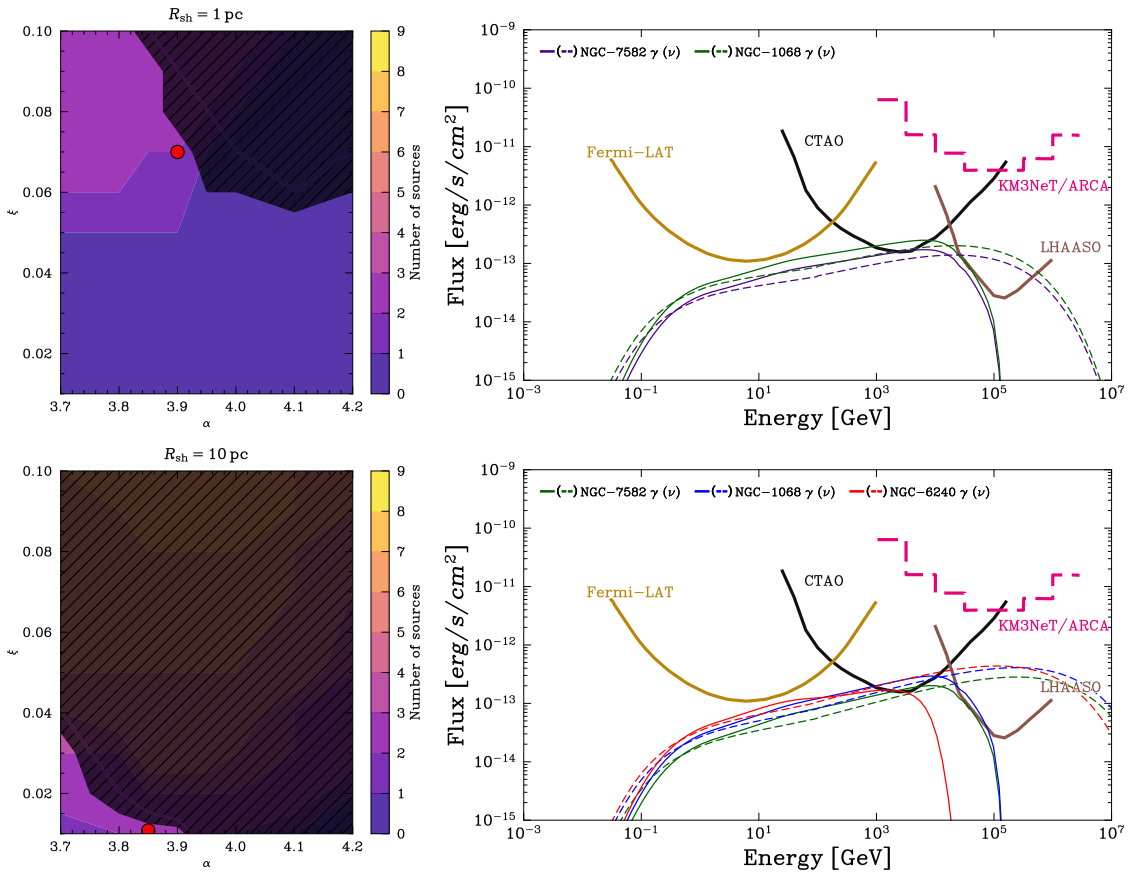

Fig. 4. Number of UFOs with a gamma-ray signal above the typical sensitivity of the CTAO (50 hours) with dark areas for parameters that lead to a *Fermi* detection. The target density is $n_0 = 10^2 \mathrm{cm}^{-3}$. Sensitivities of *Fermi*-LAT (14 years), LHAASO (5 years), and KM3NeT/ARCA (10 years) are shown.

and EBL is limited. Among these, those with outflow speeds of $v_{\mathrm{outflow}} \gtrsim 0.1$ c are particularly favorable.

It is worth noting that NGC 4151, a Seyfert galaxy with evidence of it hosting a UFO, does not appear among our TeV-detectable candidates. This results from our selection criterion that excludes all sources above *Fermi*-LAT sensitivity. However, its potential detection by *Fermi*-LAT, consistent with the properties of the UFO (Peretti et al. 2025), suggests that it could be a relevant target for further observations in the TeV domain. The case of NGC 1068 also warrants special attention. Although it is detected by *Fermi*-LAT and would thus lie above our selection threshold, the origin of its GeV emission remains ambiguous. The emission is likely a composite of AGNs and circumnuclear components in a highly opaque environment, with indications that a putative UFO could contribute to, and potentially contaminate, the observed flux (Peretti et al. 2023). In this work, we explored scenarios in which NGC 1068 would remain undetected by *Fermi*-LAT but detectable with the CTAO. Such cases imply that the GeV gamma rays observed from the host would not originate from the UFO shocks.

Having defined our sample, we now comment on the modeling of the expected emission mechanisms. In particular, we evaluate the possible leptonic contamination to the VHE spectra.

The bulk of the UFO kinetic power is expected to be thermalized at the shock. For a strong, adiabatic, non-relativistic shock ($\gamma = 5/3$), the immediate downstream temperature is given by the Rankine-Hugoniot jump conditions:

$$T_2 = \frac{3}{16}\frac{\mu m_p}{k_{\mathrm{B}}} v_s^2 \approx 1.2 \times 10^{10} \left(\frac{\mu}{0.6}\right)\left(\frac{v_s}{0.1c}\right)^2 \ \mathrm{K}, \tag{8}$$

corresponding to $k_{\mathrm{B}} T_2 \approx 1.1 \left(\frac{\mu}{0.6}\right)\left(\frac{v_s}{0.1c}\right)^2$ MeV. In a collisionless shock, this temperature primarily reflects the ion temperature immediately behind the shock, since ions receive most of the dissipated kinetic energy. The electron temperature can be parameterized as $T_e = \beta_{ep} T_p$, where $\beta_{ep} \equiv T_e/T_p \ll 1$ for high Mach-number shocks. Observations of collisionless strong shocks and kinetic simulations suggest $\beta_{ep} \sim 10^{-2}$–10^{-1}, with a conservative lower bound on the order of m_e/m_p (e.g., Ghavamian et al. 2007, 2013; Vink et al. 2015). Therefore, although shock heating converts a substantial fraction of the kinetic power into thermal energy, the resulting thermal X-ray emission (bremsstrahlung and, at lower T_e, line emission) is expected to remain subdominant relative to the intrinsic AGN X-ray luminosity. The compact AGN corona typically dominates the hard X-ray output, while the shocked region has a limited emission measure due to its thin shell geometry. In addition, circumnuclear absorption and geometrical effects can attenuate extended thermal emission. Therefore, significant shock heating does not necessarily imply a dominant or readily identifiable thermal X-ray component from the UFO shock itself.

In fact, accelerated electrons can also contribute to gamma-ray emission through inverse Compton scattering, synchrotron radiation, and bremsstrahlung. However, this contribution depends on several physical quantities, such as the magnetic-field strength, the ambient photon density, and the amount of accelerated electrons. To estimate the leptonic gamma-ray contribution, we considered an electron population following the same distribution as the protons, with $A_{\mathrm{e}} = K_{\mathrm{ep}} A$, where A is the proton normalization introduced in Eq. (3),

Table 2. Best UFO candidates and their properties associated with Fig. 3.

Sources	Distance [Mpc]	$v_{\rm outflow}$ [c]	Type
NGC 4051	8	0.128	Seyfert 1.5
MCG-5-23-16*	38	0.116	Seyfert 1.9
NGC 7582*	21	0.285	Seyfert 2
Mrk 79	94	0.091	Seyfert 1
3C 111	209	0.083	FRII
IC 5063*	47	0.311	Seyfert 2
IRAS 05054+1718(W)	77	0.176	Seyfert 1
MCG-01-24-12*	85	0.098	Seyfert 2
MCG-03-58-007*	137	0.193	Seyfert 2
Mrk 231	179	0.241	Seyfert 1
Mrk 273	162	0.265	Seyfert 2
Mrk 279	128	0.220	Seyfert 1
NGC-1068*	17	0.277	Seyfert 2
NGC 2992	34	0.298	Seyfert 1
NGC 5506	25	0.247	Seyfert 1
NGC 6240	107	0.125	Seyfert 2
PG 0844+349	274	0.211	Seyfert 1
PG 1126-041*	256	0.064	NLS 1
SWIFT J2127.4+5654	64	0.231	NLS 1

Notes. In bold are the best candidates found in the second approach illustrated in Fig. 4. Southern hemisphere sources are marked with *.

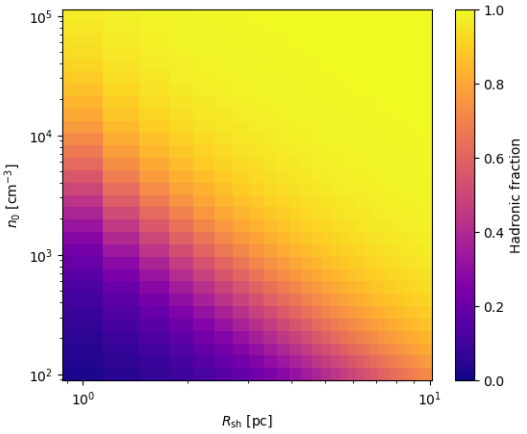

Fig. 5. Ratio of hadronic gamma rays over hadronic + leptonic gamma rays, $R_{\rm hadronic} = \frac{F_{\rm had}(>100\,{\rm GeV})}{F_{\rm had}(>100\,{\rm GeV})+F_{\rm lep}(>100\,{\rm GeV}),}$ for various values of the shock radius $R_{\rm sh}$ and ambient density n_0. In this figure, the bolometric luminosity is fixed at $L_{\rm bol} = 10^{43}$ erg/s, and the electron-to-proton ratio is set to $K_{\rm ep} = 10^{-3}$. The leptonic gamma-ray flux was computed for an inverse Compton scattering with the *Naima* code (Kafexhiu et al. 2014; Aharonian et al. 2010) assuming that the electron population follows the same energy distribution as the protons, with the normalization $K_{\rm ep}$ at 1 GeV. The AGN photon field considered is described in Sect. 2, and the maximum energy of electrons was estimated by equating the acceleration timescale to the smaller one between the loss timescale and the UFO age.

and $K_{\rm ep}$ is the electron-to-proton ratio. The value of $K_{\rm ep}$ is highly uncertain and is typically assumed to lie in the 10^{-5}–10^{-2} range (Morlino & Caprioli 2012; Park et al. 2015; Batzofin et al. 2024). As shown in Fig. 5, provided that $K_{\rm ep} < 10^{-3}$, the leptonic gamma-ray emission remains negligible compared to the hadronic signal.

For photon energies in the TeV range, Compton scattering occurs deep in the Klein-Nishina regime, where the cross-section is strongly suppressed relative to the Thomson value ($\sigma_{\rm KN} \ll \sigma_T$). Taking a representative density $n_e \sim 10^3\,{\rm cm}^{-3}$ and a characteristic size of $R \sim 1\,{\rm pc} \simeq 3\times10^{18}\,{\rm cm}$, the Thomson optical depth would be $\tau_T \sim n_e\sigma_T R \sim 2\times10^{-3}$. In the Klein-Nishina regime, the effective cross-section is further reduced by orders of magnitude, leading to $\tau_{\rm KN} \lesssim 10^{-5}$–$10^{-4}$. For the densities ($n_0 \lesssim 10^2$–$10^4\,{\rm cm}^{-3}$) and the length scales (pc) considered in this work the corresponding optical depth remains negligible ($\tau_{\rm KN} \ll 1$) . Thus, significant attenuation or energy degradation of VHE photons via Compton scattering would require electron column densities several orders of magnitude larger than those expected in UFO environments.

For the most luminous AGNs, sustaining hadronic dominance at the larger characteristic radii requires higher ambient gas densities, because the inverse Compton luminosity increases with both the electron normalization and the external photon energy density ($\propto K_{\rm ep}\,u_{\rm ph}$), whereas the hadronic component scales with the target gas density ($\propto n_0$). Conversely, for all lower luminosity AGNs considered here, hadronic dominance remains a robust expectation across the full range of ambient densities and shock radii explored: (n_0, $R_{\rm sh}$). Consequently, in the scenarios considered here, we neglected the contribution of electrons to the total gamma-ray flux.

4. Conclusions

For a list of nearby selected UFOs (Ehlert et al. 2025), we modeled particle acceleration at the strong shocks produced by these outflows and estimated the subsequent expected gamma-ray and neutrino signals. Our main conclusions are listed as follows.

1. Several UFOs are expected to be detectable by next-generation TeV gamma-ray and neutrino observatories. The number of detections depends on the physical parameters that govern particle acceleration at the UFO shocks. By exploring the parameter space, we find that harder spectra ($\alpha \lesssim 3.9$) lead to an increased number of UFOs detectable in the TeV range, while remaining undetected in the GeV range. The size of the acceleration region ($R_{\rm sh}$), the efficiency of particle acceleration ($\xi_{\rm CR}$), and the target density (n_0) all directly increase the expected number of detections.
2. In our first approach, we considered all UFOs with gamma-ray luminosities above the CTAO sensitivity in the TeV range, and we excluded those lying above the *Fermi*-LAT sensitivity. In this framework, we find that $\alpha \lesssim 3.9$ is required to ensure a TeV detection. For lower target densities ($n_0 = 10^2\,{\rm cm}^{-3}$), we further find that a cosmic-ray acceleration efficiency of $\xi_{\rm CR} \gtrsim 0.05$ is necessary.
3. In our second approach, we excluded the regions of parameter space that would lead to results in tension with the non-detection of UFOs by *Fermi*-LAT. Under these conditions, we find that a few UFOs could be detectable with the CTAO. The spectra of the detectable sources are found to be hard ($\alpha \leq 4.0$) for densities of $n_0 \geq 10^2\,{\rm cm}^{-3}$. This approach, being more stringent than the first one, leads to a reduced number of detections. Higher densities ($n_0 \gtrsim 10^3\,{\rm cm}^{-3}$) rapidly shrink the allowed regions of parameter space, ultimately resulting in no detectable sources.
4. We find that spectra harder than p^{-4} are required for detection in the VHE domain. Such spectra can, a priori, arise from several effects, including nonlinear processes due to efficient particle acceleration at the shock, or the escape of particles from the acceleration region. Radiative cooling behind the shocks, which can increase the compression

factor, could also lead to harder spectra (Cristofari 2025). The presence of clumps, which has been suggested by recent observations (Xrism Collaboration 2025), could also play a role in hardening the gamma-ray spectrum (Gabici & Aharonian 2014). A detection in the VHE domain could therefore indicate that one or more of these effects are at play.

5. Should any UFOs be detected in the VHE gamma-ray domain with hard spectra, this would indicate that additional processes not accounted for in our study are at play – for instance, the contribution of accelerated electrons. Although their role in gamma-ray production is expected to be subdominant given the high densities and magnetic fields involved, it will be investigated in a forthcoming study.
6. In both approaches, we investigated the prospects for detection with next-generation neutrino observatories, and we find that the prospects for detection with KM3NeT/ARCA over ten years are bleak.
7. The best candidates for detection in the VHE domain naturally include some of the closest UFOs in the selected sample: NGC 7582, NGC 4051, NGC 5506, NGC 2992, and NGC 6240. All of them located at $\lesssim$270 Mpc and have outflow velocities $\gtrsim$0.05 c.
8. A non-detection of UFO shocks would imply either that shocks do not form or that they are radiatively inefficient. The former would challenge current expectations for magnetohydrodynamic outflow propagation, while the latter would instead constrain the efficiency of dissipation and particle acceleration at such shocks. In this sense, non-detections primarily inform the microphysics of interactions in the UFO environment rather than implying the absence of shocks.
9. Comparing the predictions of our model with future gamma-ray observations of the UFO population will offer a novel approach to probing particle acceleration in these outflows. Furthermore, the global properties of the UFO population – such as source count, luminosity distribution, distances, and spectral indices – can help place tighter constraints on particle-acceleration mechanisms at strong, sub-relativistic collisionless shocks.

In a follow-up investigation, we plan to explore the multiwavelength impact of leptons in UFOs and to undertake a dedicated study of potential and nearby UFO hosts detected in gamma rays by *Fermi*-LAT such as NGC 1068 and NGC 4151. It is important to note that NGC 1068 has been proposed as a potential UFO host (Yamada et al. 2024), but this interpretation remains under debate and lacks definitive evidence.

Acknowledgements. This work was supported by the PSL Starting Grant GALAPAGOS. EP acknowledges economic support from INAF through "Assegni di ricerca per progetti di ricerca relativi a CTA e precursori".

References

Acharya, B. S, et al. 2018, Cherenkov Telescope Array Consortium, https://doi.org/10.1142/10986
Aartsen, M. G., Abbasi, R., Ackermann, M., et al. 2021, J. Phys. G Nucl. Phys., 48, 060501
Abdollahi, S., Acero, F., Ackermann, M., et al. 2020, ApJS, 247, 33
Aharonian, F. A., Kelner, S. R., & Prosekin, A. Y. 2010, Phys. Rev. D, 82, 043002
Aiello, S., Albert, A., Alshamsi, M., et al. 2024, Astropart. Phys., 162, 102990
Ajello, M., Baldini, L., Ballet, J., et al. 2021, ApJ, 921, 144
Ajello, M., Murase, K., & McDaniel, A. 2023, ApJ, 954, L49
Amato, E., & Blasi, P. 2005, MNRAS, 364, L76
Atwood, W. B., Abdo, A. A., Ackermann, M., et al. 2009, ApJ, 697, 1071
Batzofin, R., Cristofari, P., Egberts, K., Steppa, C., & Meyer, D. M. A. 2024, A&A, 687, A279
Cappi, M., Tombesi, F., Bianchi, S., et al. 2009, A&A, 504, 401
Caprioli, D., Haggerty, C. C., & Blasi, P. 2020, ApJ, 905, 2
Chartas, G., Brandt, W. N., Gallagher, S. C., & Garmire, G. P. 2002, ApJ, 579, 169
Chartas, G., Saez, C., Brandt, W. N., Giustini, M., & Garmire, G. P. 2009, ApJ, 706, 644
Chartas, G., Cappi, M., Vignali, C., et al. 2021, ApJ, 920, 24
Chevalier, R. A., & Clegg, A. W. 1985, Nature, 317, 44
Cristofari, P. 2025, A&A, 704, A213
Cristofari, P., Blasi, P., & Caprioli, D. 2022, ApJ, 930, 28
Ehlert, D., Oikonomou, F., & Peretti, E. 2025, MNRAS, 539, 2435
Eichmann, B., Oikonomou, F., Salvatore, S., Dettmar, R.-J., & Tjus, J. B. 2022, ApJ, 939, 43
Faucher-Giguère, C.-A., & Quataert, E. 2012, MNRAS, 425, 605
Franceschini, A., & Rodighiero, G. 2017, A&A, 603, A34
Fukumura, K., Kazanas, D., Contopoulos, I., & Behar, E. 2010, ApJ, 715, 636
Fukumura, K., Tombesi, F., Kazanas, D., et al. 2014, ApJ, 780, 120
Gabici, S., & Aharonian, F. A. 2014, MNRAS, 445, L70
Ghavamian, P., Laming, J. M., & Rakowski, C. E. 2007, ApJ, 654, L69
Ghavamian, P., Schwartz, S. J., Mitchell, J., Masters, A., & Laming, J. M. 2013, Space Sci. Rev., 178, 633
Gianolli, V. E., Bianchi, S., Petrucci, P. O., et al. 2024, A&A, 687, A235
Gofford, J., Reeves, J. N., Tombesi, F., et al. 2013, MNRAS, 430, 60
Gu, L., Fukumura, K., Kaastra, J., et al. 2025, A&A, 704, A146
Hillas, A. M. 1984, ARA&A, 22, 425
Jiang, Y.-F., Stone, J. M., & Davis, S. W. 2014, ApJ, 796, 106
Kafexhiu, E., Aharonian, F., Taylor, A. M., & Vila, G. S. 2014, Phys. Rev., D, 90
Kelner, S. R., Aharonian, F. A., & Bugayov, V. V. 2006, Phys. Rev. D, 74, 034018
Khangulyan, D., Aharonian, F. A., & Kelner, S. R. 2014, ApJ, 783, 100
King, A., & Pounds, K. 2015, ARA&A, 53, 115
Laha, S., Smith, R., Tzanavaris, P., et al. 2019, BAAS, 51, 75
Lamastra, A., Fiore, F., Guetta, D., et al. 2016, A&A, 596, A68
Lamastra, A., Tavecchio, F., Romano, P., Landoni, M., & Vercellone, S. 2019, Astropart. Phys., 112, 16
Lenain, J.-P., Ricci, C., Türler, M., Dorner, D., & Walter, R. 2010, A&A, 524, A72
Malkov, M. A., & Drury, L. O. 2001, Rep. Prog. Phys., 64, 429
Marconi, A., Risaliti, G., Gilli, R., et al. 2004, MNRAS, 351, 169
Matzeu, G. A., Brusa, M., Lanzuisi, G., et al. 2023, A&A, 670, A182
Mestici, S., Tombesi, F., Gaspari, M., Piconcelli, E., & Panessa, F. 2024, MNRAS, 532, 3036
Miniati, F., Jones, T. W., & Ryu, D. 1999, ApJ, 517, 242
Morlino, G., & Caprioli, D. 2012, A&A, 538, A81
Mullaney, J. R., Alexander, D. M., Goulding, A. D., & Hickox, R. C. 2011, MNRAS, 414, 1082
Murase, K., Karwin, C. M., Kimura, S. S., Ajello, M., & Buson, S. 2024, ApJ, 961, L34
Neronov, A., & Semikoz, D. 2020, Phys. Rev., D, 102
Nims, J., Quataert, E., & Faucher-Giguère, C.-A. 2015, MNRAS, 447, 3612
Padovani, P., Resconi, E., Ajello, M., et al. 2024, Nat. Astron., 8, 1077
Park, J., Caprioli, D., & Spitkovsky, A. 2015, Phys. Rev. Lett., 114, 085003
Peretti, E., Lamastra, A., Saturni, F. G., et al. 2023, MNRAS, 526, 181
Peretti, E., Peron, G., Tombesi, F., et al. 2025, JCAP, 2025, 013
Pounds, K. A., Reeves, J. N., King, A. R., et al. 2003, MNRAS, 345, 705
Reeves, J. N., O'Brien, P. T., & Ward, M. J. 2003, ApJ, 593, L65
Ricci, C., & Trakhtenbrot, B. 2023, Nat. Astron., 7, 1282
Salvatore, S., Eichmann, B., Rodrigues, X., Dettmar, R.-J., & Becker Tjus, J. 2024, A&A, 687, A139
Silk, J., & Rees, M. J. 1998, A&A, 331, L1
Tombesi, F., Cappi, M., Reeves, J. N., et al. 2010, A&A, 521, A57
Tombesi, F., Cappi, M., Reeves, J. N., & Braito, V. 2012, MNRAS, 422, L1
Tombesi, F., Tazaki, F., Mushotzky, R. F., et al. 2014, MNRAS, 443, 2154
Vink, J., Broersen, S., Bykov, A., & Gabici, S. 2015, A&A, 579, A13
Weaver, R., McCray, R., Castor, J., Shapiro, P., & Moore, R. 1977, ApJ, 218, 377
Xrism Collaboration (Audard, M., et al.) 2025, Nature, 641, 1132
Xu, Y., Gallo, L. C., Hagino, K., et al. 2025, PASJ, 77, S223
Yamada, S., Kawamuro, T., Mizumoto, M., et al. 2024, ApJS, 274, 8
Yoast-Hull, T. M., Gallagher, J. S., III, Zweibel, E. G., & Everett, J. E. 2014, ApJ, 780, 137
Zavala, R. T., & Taylor, G. B. 2004, ApJ, 612, 749
Zirakashvili, V. N., & Ptuskin, V. S. 2008, in AIP Conf. Ser., eds. F. A. Aharonian, W. Hofmann, & F. Rieger (AIP), 1085, 336